AIChE WILEY InterScience DISCOVER SOMETHING GREAT

FLUID MECHANICS AND TRANSPORT PHENOMENA

Theoretical Analysis of Laminar Flow of Power-Law Fluids in Coiled Tubing

Y. Zhou and S. N. Shah
Well Construction Technology Center, Mewbourne School of Petroleum and Geological Engineering, University of Oklahoma, Norman, OK 73069

DOI 10.1002/aic.11246
Published online July 9, 2007 in Wiley InterScience (www.interscience.wiley.com).

*A comprehensive theoretical study of the flow of power-law fluid in coiled tubing by using the boundary layer approximation method is presented. First, a boundary layer approximation analysis was applied to the governing equations of continuity and motion of a power law fluid in the curved tubing flow geometry. Momentum integral equations for the boundary layer flow were then derived and solved numerically. The resulting solutions of the velocity field were used to develop a new friction factor correlation in terms of generalized Dean number, coiled tubing curvature ratio, and flow behavior index of the power law fluid model. The new correlation of this study and a previous correlation by Mashelkar and Devarajan were evaluated using experimental data obtained from full-scale coiled tubing flow experiments. An excellent agreement was found between the new correlation and the experimental results. The Mashelkar and Devarajan correlation did not result in any acceptable agreement with the experimental data, nor did it match the Ito correlation for the limiting case of Newtonian fluids (*n *= 1). This work extends the range of applicability of the new correlation to fluids with flow behavior indices as low as 0.25, which would cover most fluids used for coiled tubing operations in the oil and gas industry as well as fluids used in other industries.* © 2007 American Institute of Chemical Engineers *AIChE J,* 53: 2210–2220, 2007

Keywords: coiled tubing, non-Newtonian fluid, drilling/completion, stimulation*, friction pressure, curvature effect*

Introduction

Fluid flow in coiled tubing (CT) is featured by the secondary flows of the spiral form that are superimposed on the axial primary flow, which causes greater flow resistance than in straight pipes. The first theoretical study of fluid flow in curved pipes was made by Dean,[1,2] who, using a successive approximation method, obtained an analytical solution for fluid flow in a small-curvature pipe. He also showed that the dynamic similarity of the flow depends on a nondimensional parameter that was later called Dean number. The preferred definition of Dean number is: $N_{De} = N_{Re}(a/R)^{1/2}$, where a and R are the radii of the pipe and the coil, and N_{Re} is the Reynolds number. The Dean number provides a fundamental parameter in developing flow resistance correlations for flow in curved pipes. Since the pioneering work of Dean,[1,2] the flow behavior of Newtonian fluids in coiled pipes has been studied extensively, both theoretically and experimentally.[3] The various theoretical methods can be roughly grouped as analytical solutions for small Dean numbers, numerical methods for intermediate Dean numbers, and the boundary layer approximation methods for large Dean numbers. Compared with its counterpart of Newtonian fluid, the flow of non-Newtonian fluid in coiled pipes has remained relatively unstudied.[3]

Correspondence concerning this article should be addressed to Y. Zhou at yunxuzhou@yahoo.com.

© 2007 American Institute of Chemical Engineers

CT has been successfully used in well drilling, completion, stimulation, and many other operations in the petroleum industry. The use of CT in these applications unexceptionally involves pumping fluids (typically non-Newtonian fluids) through them. Yet, correlations that can be used to accurately predict the frictional pressure losses and power requirement for pumping these non-Newtonian fluids through CT are not available.

The objective of this study is to theoretically investigate the flow problem of non-Newtonian fluid in CT and to develop correlations for predicting frictional pressure losses.

Considering that the flow conditions encountered in most CT operations fall in the range of large Dean number, the boundary layer approximation approach was adopted. According to the theory of this approach, the pipe cross-section can be divided into two regions: the central inviscid core and the thin boundary layer surrounding it where the viscous effect is significant. This concept has been supported by experiments and numerical simulations,[4–7] which showed that at large Dean number, the secondary flow is essentially confined to a thin boundary layer near the tubing wall. Studies of this category include Adler,[4] Barua,[8] Mori and Nakayama,[9] Ito,[10] and Mashelkar and Devarajan.[11] The approach of Ito[10] and Mashelkar and Devarajan[11] was closely followed in this study.

A new friction factor correlation has been developed based on the numerical solutions of the velocity field from the boundary layer approximation analysis. The new correlation was then verified using the experimental data from full-scale CT flow experiments. A previous correlation by Mashelkar and Devarajan[11] was also evaluated with the experimental data and the Ito[10] correlation.

Mathematical Formulation

Governing equations

The toroidal coordinate system, shown in Figure 1, is used to represent the flow geometry of fluid flow in CT. Here, u, v, and w represent velocity components in the directions of r, θ, and ϕ, respectively. a and R are the radii of the CT and the tubing reel, respectively. The ratio, a/R, is often called the curvature ratio.

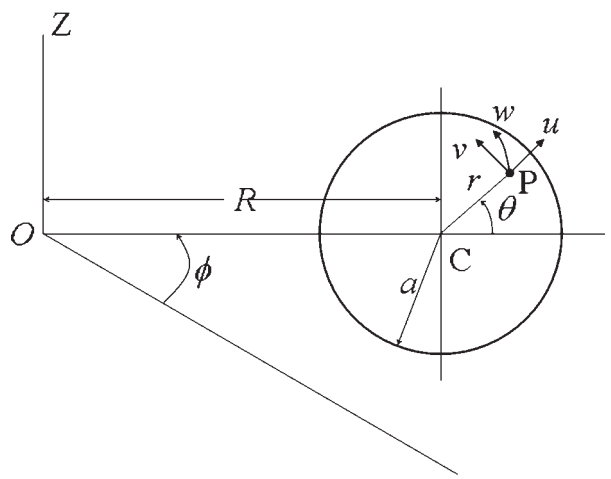

Figure 1. Toroidal coordinate system.

Several assumptions have been made and they are as follows:

(a) The flow is steady and fully-developed laminar flow;
(b) The curvature ratio (a/R) is small;
(c) The pitch of the CT is negligible;
(d) The Dean number is large, and therefore, only viscous forces are important in a thin boundary layer near the tubing wall, and the flow outside the boundary layer is influenced by the inertial and pressure forces alone.
(e) The rheological behavior of the fluid can be described by an Ostwald-de Waele power law model.

The equations of motion and continuity are as follows:[11]

$$\rho\left(u\frac{\partial u}{\partial r}+\frac{v}{r}\frac{\partial u}{\partial \theta}-\frac{v^2}{r}-\frac{w^2\cos\theta}{R}\right) = -\frac{\partial p}{\partial r}-\left(\frac{\partial \tau_{rr}}{\partial r}+\frac{1}{r}\frac{\partial \tau_{r\theta}}{\partial \theta}+\frac{\tau_{rr}-\tau_{\theta\theta}}{r}\right) \quad (1)$$

$$\rho\left(u\frac{\partial v}{\partial r}+\frac{v}{r}\frac{\partial v}{\partial \theta}+\frac{uv}{r}+\frac{w^2\sin\theta}{R}\right) = -\frac{1}{r}\frac{\partial p}{\partial \theta}-\left(\frac{\partial \tau_{r\theta}}{\partial r}+\frac{1}{r}\frac{\partial \tau_{\theta\theta}}{\partial \theta}+\frac{2}{r}\tau_{r\theta}\right) \quad (2)$$

$$\rho\left(u\frac{\partial w}{\partial r}+\frac{v}{r}\frac{\partial w}{\partial \theta}\right) = -\frac{1}{R}\frac{\partial p}{\partial \phi}-\left(\frac{\partial \tau_{r\phi}}{\partial r}+\frac{1}{r}\frac{\partial \tau_{\theta\phi}}{\partial \theta}+\frac{2\tau_{r\phi}\sin\theta}{R}\right) \quad (3)$$

$$\frac{\partial u}{\partial r}+\frac{u}{r}+\frac{1}{r}\frac{\partial v}{\partial \theta}=0 \quad (4)$$

$$-\frac{\partial p}{\partial \phi}=C \quad (5)$$

where ρ is fluid density, p is pressure, and τ_{rr}, $\tau_{\theta\theta}$, $\tau_{r\theta}$, $\tau_{r\phi}$, and $\tau_{\theta\phi}$ are stress terms. The second index of these stresses indicates the direction of stress and the first index indicates the plane of the stress. For example, $\tau_{r\phi}$ indicates stress in the direction of ϕ on a plane that is normal to direction of r.

The overall flow through the tubing cross-section can be divided into two regions: a central inviscid core and a thin boundary layer adjacent to the tubing wall, schematically shown in Figure 2. The central part of the fluid will be driven towards the outer wall because of the centrifugal force. The fluid entering the boundary layer will be pushed back along the wall toward the inner side. This will result in the double vortical motion in the cross-section of the tubing.

Flow equations outside the boundary layer

In the region outside the boundary layer, the axial velocity distribution is more uniform than in the boundary layer, and therefore, the secondary velocity components, u and v, may be small compared with the primary component w, i.e., u and $v \ll w$. Considering that the viscous effect can be neglected in the core region,[8–10] Eqs. 1–3 reduce to:

$$-\frac{w^2\cos\theta}{R}=-\frac{1}{\rho}\frac{\partial p}{\partial r} \quad (6)$$

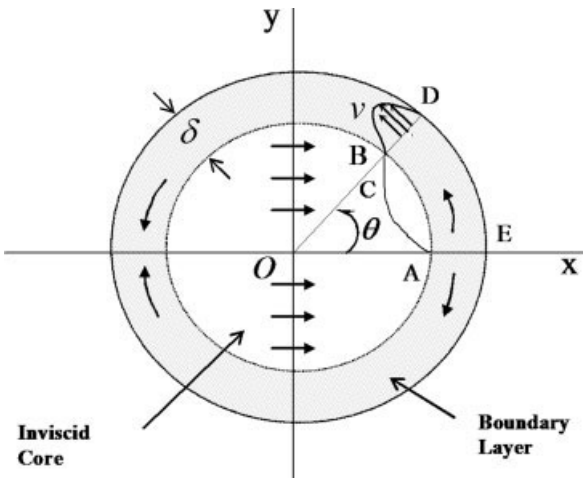

Figure 2. Flow model showing the inviscid core and boundary layer.

$$\frac{w^2 \sin\theta}{R} = -\frac{1}{\rho r}\frac{\partial p}{\partial \theta} \tag{7}$$

$$u\frac{\partial w}{\partial r} + \frac{v}{r}\frac{\partial w}{\partial \theta} = \frac{C}{\rho R} \tag{8}$$

Noting that

$$\sin\theta\frac{\partial}{\partial r} + \frac{\cos\theta}{r}\frac{\partial}{\partial \theta} = \frac{\partial}{\partial y} \tag{9}$$

and if p is eliminated from Eqs. 6 and 7, we have

$$\frac{\partial w}{\partial y} = 0 \tag{10}$$

which gives

$$w = F(x) \tag{11}$$

where F is an arbitrary function of x.

From Eq. 4, we can introduce a stream function ψ so that

$$u = \frac{1}{r}\frac{\partial \psi}{\partial \theta}, \quad v = -\frac{\partial \psi}{\partial r} \tag{12}$$

Inserting Eqs. 11 and 12 into Eq. 8 and integrating, we have

$$\psi = \frac{Cy}{\rho R F'(x)} + \text{const.} \tag{13}$$

where $F'(x) = dF/dx$. The function $F(x)$ will be determined later from the condition of continuity of the secondary flow between the core and the boundary layer.

Boundary layer equations

In the boundary layer, the axial velocity component w will be reduced from a value, w_1 (here the subscript 1 denotes the edge of the boundary layer) at the edge of the boundary layer to zero at the wall (no-slip boundary). Therefore, the secondary flow component v becomes comparable with w. To obtain simplified equations for the boundary layer, we conduct order of magnitude analysis:

$$u \sim O(\delta); \quad v, w \sim O(1); \quad \frac{\partial}{\partial r} \sim O(\delta^{-1}); \quad \frac{\partial}{\partial \theta}, \frac{\partial}{\partial \phi} \sim O(1) \tag{14}$$

where δ is the boundary layer thickness.

Equations 1–4 then reduce to:[11,12]

$$-\frac{v^2}{a} - \frac{w^2 \cos\theta}{R} = -\frac{1}{\rho}\frac{\partial p}{\partial r} \tag{15}$$

$$u\frac{\partial v}{\partial r} + \frac{v}{a}\frac{\partial v}{\partial \theta} + \frac{w^2 \sin\theta}{R} = -\frac{1}{\rho a}\frac{\partial p}{\partial \theta} - \frac{1}{\rho}\frac{\partial \tau_{r\theta}}{\partial r} \tag{16}$$

$$u\frac{\partial w}{\partial r} + \frac{v}{a}\frac{\partial w}{\partial \theta} = -\frac{1}{\rho R}\frac{\partial p}{\partial \phi} - \frac{1}{\rho}\frac{\partial \tau_{r\phi}}{\partial r} \tag{17}$$

$$\frac{\partial u}{\partial r} + \frac{1}{a}\frac{\partial v}{\partial \theta} = 0 \tag{18}$$

Next, Eqs. 16 and 17 will be further simplified. Equation 15 indicates that the pressure variation over the boundary layer is only of the order δ, and can be neglected. Therefore, we have $p(r,\theta,\phi) = p_1(\theta,\phi)$ where the subscript 1 denotes the edge of the boundary layer. Hence, from Eq. 7,

$$\frac{\partial p}{\partial \theta} = -\rho\frac{a}{R}w_1^2 \sin\theta \tag{19}$$

Equation 16 then becomes:

$$u\frac{\partial v}{\partial r} + \frac{v}{a}\frac{\partial v}{\partial \theta} = \frac{w_1^2 - w^2}{R}\sin\theta - \frac{1}{\rho}\frac{\partial \tau_{r\theta}}{\partial r} \tag{20}$$

Further order of magnitude analysis[10,11] shows that the first term on the right hand side of Eq. 17 can be neglected because of its small magnitude and hence Eq. 17 can be simplified as:

$$u\frac{\partial w}{\partial r} + \frac{v}{a}\frac{\partial w}{\partial \theta} = -\frac{1}{\rho}\frac{\partial \tau_{r\phi}}{\partial r} \tag{21}$$

If a power law rheological model ($\tau = K\dot{\gamma}^n$) is assumed, Eqs. 20 and 21 can be written as:

$$u\frac{\partial v}{\partial r} + \frac{v}{a}\frac{\partial v}{\partial \theta} = \frac{w_1^2 - w^2}{R}\sin\theta + \frac{K}{\rho}\frac{\partial}{\partial r}\left[-\left(\frac{\partial w}{\partial r}\right)^{n-1}\left(\frac{\partial v}{\partial r}\right)\right] \tag{22}$$

$$u\frac{\partial w}{\partial r} + \frac{v}{a}\frac{\partial w}{\partial \theta} = \frac{K}{\rho}\frac{\partial}{\partial r}\left(-\frac{\partial w}{\partial r}\right)^n \tag{23}$$

where n and K are the flow behavior index and consistency index of the power law model. In Eqs. 22 and 23, we neglected the effect of $(\partial v/\partial r)$ on the total shear rate, since $(\partial v/\partial r)^2 \ll (\partial w/\partial r)^2$ for $a/R \ll 1$.

For boundary conditions, we shall have approximately[10,11]

$$r = a - \delta, \quad v \cong 0, \quad \frac{\partial v}{\partial r} \cong 0 \tag{24}$$

$$r = a - \delta,\ w = w_1,\ \left(\frac{\partial w}{\partial r}\right)_1 \cong 0 \tag{25}$$

Continuity of the secondary flow

In Figure 2, let A and B be the points on the outer edge of the boundary layer. Using Eq. 13, the flux across a curve ACB drawn outside the boundary layer is:

$$\int_A^B d\Psi = \Psi_B - \Psi_A = \frac{Ca \sin\theta}{\rho R F'(x)} \tag{26}$$

Across AE, $v = 0$ for reasons of symmetry. Across BD, the flux is $\int_0^\delta v d\xi$, where

$$\xi = a - r \tag{27}$$

We have then

$$\frac{Ca \sin\theta}{\rho R F'(x)} = \int_0^\delta v d\xi \tag{28}$$

Considering $x \approx a \cos\theta$ in the thin boundary layer, we have

$$F'(x) = \frac{dw}{dx} = -\frac{1}{a \sin\theta}\frac{dw_1}{d\theta} \tag{29}$$

From Eqs. 28 and 29, it follows that

$$\frac{dw_1}{d\theta} = -\frac{Ca^2 \sin^2\theta}{\rho R \int_0^\delta v d\xi} \tag{30}$$

Considering the force balance for a cylindrical volume of length $Rd\phi$ and radius a, we have

$$2\int_0^\pi \int_0^a \left[p - \left(p + \frac{\partial p}{\partial \phi} d\phi\right)\right] r dr d\theta = Rd\phi 2a \int_0^\pi \tau_{r\phi} d\theta \tag{31}$$

Hence,

$$C = -\frac{\partial p}{\partial \phi} = \frac{2R}{\pi a}\int_0^\pi \tau_{r\phi} d\theta \tag{32}$$

Boundary layer momentum integrals

Integrating Eq. 22 over the boundary layer thickness δ and using Eqs. 18 and 24, we have

$$\frac{a}{\rho}\tau_{r\theta}|_{\xi=0} = -\frac{d}{d\theta}\int_0^\delta v^2 d\xi + \frac{a}{R}\sin\theta \int_0^\delta (w_1^2 - w^2) d\xi \tag{33}$$

Similarly from Eq. 23, we have

$$\frac{a}{\rho}\tau_{r\phi}|_{\xi=0} = w_1 \frac{d}{d\theta}\int_0^\delta v d\xi - \frac{d}{d\theta}\int_0^\delta vw d\xi \tag{34}$$

Application of the Pohlhausen method

The Pohlhausen's approximation method is followed for solving the velocity distribution in the boundary layer. We are looking for solutions of v and w in the boundary layer that satisfy the following boundary conditions:

$$\xi = 0\colon\ v = 0,\ -\frac{w_1^2 \sin\theta}{R} = \frac{K}{\rho}\frac{\partial}{\partial r}\left[\left(-\frac{\partial w}{\partial r}\right)^{n-1}\left(\frac{\partial v}{\partial r}\right)\right] \tag{35}$$

$$\xi = \delta\colon\ v = 0,\ \frac{\partial v}{\partial \xi} = 0 \tag{36}$$

$$\xi = 0\colon w = 0, \frac{\partial^2 w}{\partial \xi^2} = 0 \tag{37}$$

$$\xi = \delta\colon w = w_1, \frac{\partial w}{\partial \xi} = 0 \tag{38}$$

The earlier conditions can be satisfied by the following velocity profiles:[11]

$$v = \left(\frac{2}{3}\right)^{n-1}\frac{\rho \sin\theta}{KR}\delta^{n+1} w_1^{3-n} g(\eta) + Sh(\eta) \tag{39}$$

and

$$w = w_1 k(\eta) \tag{40}$$

where,

$$g(\eta) = \frac{1}{6}\left(2\eta - 3\eta^2 + \eta^4\right) \tag{41}$$

$$h(\eta) = \frac{1}{6}\left(\eta - 3\eta^3 + 2\eta^4\right) \tag{42}$$

$$k(\eta) = \frac{1}{2}\left(3\eta - \eta^3\right) \tag{43}$$

and

$$\eta = \frac{\xi}{\delta} \tag{44}$$

S can be considered as a shape factor of v-velocity component and is a function of angle θ. Now our task becomes solving for δ, w_1, and S from the two boundary layer momentum integral equations (Eqs. 33 and 34) and the boundary layer continuity equation (Eq. 30) as well as the boundary conditions.

To reduce Eqs. 33, 34, and 30 to nondimensional form, the following dimensionless variables are defined:

$$\delta_o = \left(\frac{\delta}{a}\right) D_{e0}{}^{1/(n+1)} \tag{45}$$

$$S_o = \frac{S}{w_{10}}(a/R)^{-1/2} \tag{46}$$

$$w_o = \frac{w_1}{w_{10}} \tag{47}$$

where,

$$D_{e0} = N'_{\mathrm{Reg}}\sqrt{a/R} \tag{48}$$

and w_{10} is the value of w_1 at $\theta = 0$. N'_{Reg} is defined as:

$$N'_{\mathrm{Reg}} = \frac{(a)^n w_{10}^{2-n}\rho}{K} \tag{49}$$

Since the specific expressions for $g(\eta)$, $h(\eta)$, and $k(\eta)$ are already given in Eqs. 41–43, the integrals and the terms of $\tau_{r\theta}|_{\xi=0}$ and $\tau_{r\phi}|_{\xi=0}$ in Eqs. 33 and 34 can be evaluated. The final differential equations in a nondimensional form are obtained as the following:

$$\frac{d}{d\theta}\left[\frac{17}{315}\left(\frac{2}{3}\right)^{2(n-1)}\delta_o^{2(n+1)+1}w_o^{2(3-n)}\sin^2\theta + \frac{101}{1260}\left(\frac{2}{3}\right)^{n-1}\delta_o^{n+2}w_o^{3-n}S_o\sin\theta + \frac{19}{630}\delta_o S_o^2\right] = 6\left[\frac{38}{35}\delta_o w_o^2\sin\theta - \left(\frac{2}{3}\right)^{1-n}\frac{S_o w_o^{n-1}}{\delta_o^n}\right] \tag{50}$$

$$w_o\frac{d}{d\theta}\left[\frac{1}{3}\left(\frac{2}{3}\right)^{n-1}\delta_o^{n+2}w_o^{3-n}\sin\theta + \frac{S_o\delta_o}{4}\right] - \frac{d}{d\theta}\left[\frac{3}{16}\left(\frac{2}{3}\right)^{n-1}\delta_o^{n+2}w_o^{4-n}\sin\theta + \frac{25}{168}\delta_o w_o S_o\right] = 10\left(\frac{2}{3}\right)^{-n}\frac{w_o^n}{\delta_o^n} \tag{51}$$

$$\frac{dw_o}{d\theta} = -\frac{120\alpha\sin^2\theta}{\left[4\left(\frac{2}{3}\right)^{n-1}\delta_o^{n+2}w_o^{3-n}\sin\theta + 3S_o\delta_o\right]} \tag{52}$$

where,

$$\alpha = \frac{2}{\pi}\left(\frac{2}{3}\right)^{-n}\int_0^{\pi}\frac{w_o^n}{\delta_o^n}d\theta \tag{53}$$

Solution Procedure

The task now becomes solving for δ_o, w_o, and S_o as function of θ from the coupled, nonlinear ordinary differential equations (Eqs. 50–53). This can be accomplished by integrating Eqs. 50–52 with the angle θ in the range of $0-\pi$. A Runge–Kutta scheme was used to solve the system of ordinary differential equations. The initial condition (at $\theta = 0$) was determined following Ito's approach.[10] In the neighborhood of $\theta = 0$, let

$$\delta_o = \delta_{o0}\left(1 + \delta_{o2}\theta^2 + \cdots\right) \tag{54}$$

$$S_o = S_{o1}\theta\left(1 + S_{o3}\theta^2 + \cdots\right) \tag{55}$$

$$w_o = 1 + w_{o2}\theta^2 + \cdots \tag{56}$$

Substituting these expansions into Eqs. 50 and 51 leads to two equations for δ_{o0} and S_{o1} with the flow behavior index (n) of the power law model as a parameter.

$$68\left(\frac{2}{3}\right)^{2(n-1)} + 101\left(\frac{2}{3}\right)^{n-1}\frac{S_{o1}}{\delta_{o0}^{n+1}} + 38\left(\frac{S_{o1}}{\delta_{o0}^{n+1}}\right)^2 = \frac{108}{\delta_{o0}^{2(n+1)}}\left[38 - 35\left(\frac{2}{3}\right)^{1-n}\frac{S_{o1}}{\delta_{o0}^{n+1}}\right] \tag{57}$$

$$49\left(\frac{2}{3}\right)^{n-1} + 34\frac{S_{o1}}{\delta_{o0}^{n+1}} = 3360\left(\frac{2}{3}\right)^{-n}\frac{1}{\delta_{o0}^{2(n+1)}} \tag{58}$$

Therefore, for a given value of n, the initial condition can be determined by solving the earlier two equations. To evaluate α from numerical solutions of w_o and δ_o, the Simpson's rule was employed for the numerical integration in Eq. 53.

Note that to solve for δ_o, w_o, and S_o numerically, the value of α must be known. But Eq. 53 indicates that α depends on the solutions of δ_o and w_o. Therefore, a trial-and-error method is needed. First, with an assumed value of α, Eqs. 50–52 were numerically integrated. Then δ_o and w_o thus determined were substituted into Eq. 53 and a new value of α was found. The calculation procedure was repeated until the difference between the assumed value and the calculated value of α satisfied a specified convergence criterion.

Once the solutions for dimensionless variables δ_o, w_o, and S_o are obtained, the velocity field both in the boundary layer and the central core can be defined by using Eqs. 11–13, 29, 30, 39, 40, and 45–47. Friction factor correlations can then be developed, as will be shown later.

Results and Discussion

Numerical solutions of Eqs. 50–52

Numerical solutions of the governing equations, Eqs. 50–52, were obtained for a wide range of flow behavior index (n)—from 0.25 to 1.0 in steps of 0.05. Figures 3–5 show the solutions of δ_o, S_o, W_o for $n = 1.0$, 0.9, 0.7, 0.5, and 0.3, respectively. To check the accuracy of the calculation method, the results of the Newtonian fluid ($n = 1$) were compared with the Ito's solution. Our results were in excellent agreement with Ito's result.

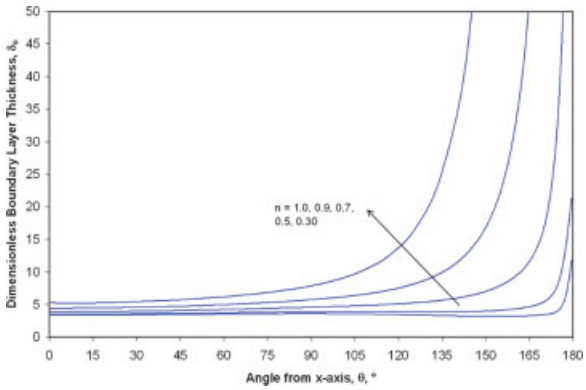

Figure 3. Dimensionless boundary layer thickness, δ_o.

[Color figure can be viewed in the online issue, which is available at www.interscience.wiley.com.]

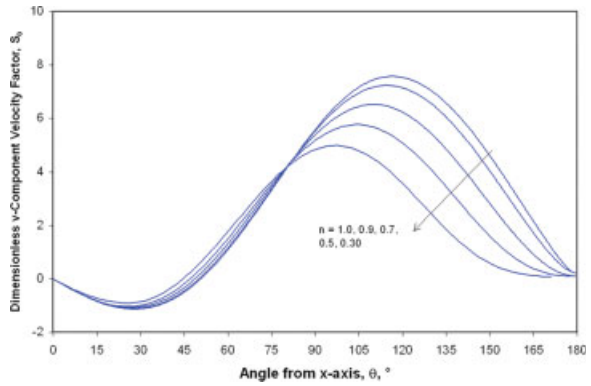

Figure 4. Dimensionless v-velocity component factor, S_o.

[Color figure can be viewed in the online issue, which is available at www.interscience.wiley.com.]

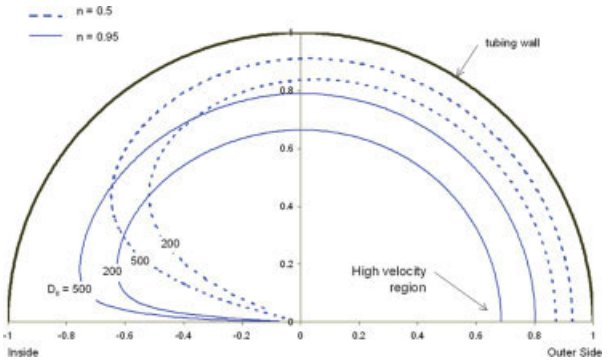

Figure 6. Effects of flow behavior index and Dean number on the profiles of the boundary layer thickness.

[Color figure can be viewed in the online issue, which is available at www.interscience.wiley.com.]

Figure 6 shows the profiles of boundary layer thickness (normalized as δ/a) for flow behavior index $n = 0.95$ and 0.5, and Dean number $D_e = 200$ and 500, respectively. It can be seen that as the Dean number increases, the boundary layer becomes thinner. As n decreases from 0.95 to 0.5, the boundary layer adjacent to the outer wall becomes thinner, while it is becoming thicker at the inner side of the tubing wall. This implies that as the flow behavior index n decreases, the high velocity will shift more and more toward the outer wall, whereas the cross-sectional area near the inner wall will contribute less and less to the total flux.

Development of new friction factor correlation

The Fanning friction factor, f, can be defined as

$$f = \frac{\left[-\left(\frac{\partial p}{R\partial\phi}\right)\right](2a)}{4\left(\frac{1}{2}\rho v_m^2\right)} \tag{59}$$

The pressure gradient ($\partial p/\partial\phi$) is related to the flow field through Eq. 32. Following the Ito[10] and Mashelkar and Devarajan's[11] approach, the following equation can be derived from Eqs. 59 and 32:

$$f = 2^{n/(n+1)}\alpha D_e^{-1/(n+1)}\left(\frac{a}{R}\right)^{1/2}\left(\frac{v_m}{w_{10}}\right)^{-3n/(n+1)} \tag{60}$$

where α is determined from Eq. 53.

Therefore, if (v_m/w_{10}) is known, the Fanning friction factor can be calculated. In fact, (v_m/w_{10}) can be determined from the numerical solution of fluid velocities as follows.

The total flow rate, Q, through the tubing cross section can be calculated by integrating velocity in the core region and the boundary layer region:

$$Q = 2\int_{-a}^{a} w_1\sqrt{a^2 - x^2}dx - 2a\int_0^{\pi}\int_0^{\delta}(w_1 - w)d\xi d\theta \tag{61}$$

The mean axial velocity is expressed as:[10]

$$v_m = \frac{Q}{\pi a^2} = \frac{2}{\pi}\int_0^{\pi} w_1 \sin^2\theta d\theta - \frac{3}{4\pi a}\int_0^{\pi} w_1\delta d\theta \tag{62}$$

This can be written in nondimensional form as

$$\frac{v_m}{w_{10}} = \frac{2}{\pi}\int_0^{\pi} w_o \sin^2\theta d\theta - \frac{3}{\pi}2^{-(n+2)/(n+1)}D_e^{-1/(n+1)}\left(\frac{v_m}{w_{10}}\right)^{(2-n)/(n+1)}\int_0^{\pi} w_o\delta_o d\theta$$

or

$$\frac{v_m}{w_{10}} = \beta - \gamma D_e^{-1/(n+1)}\left(\frac{v_m}{w_{10}}\right)^{(2-n)/(1+n)} \tag{63}$$

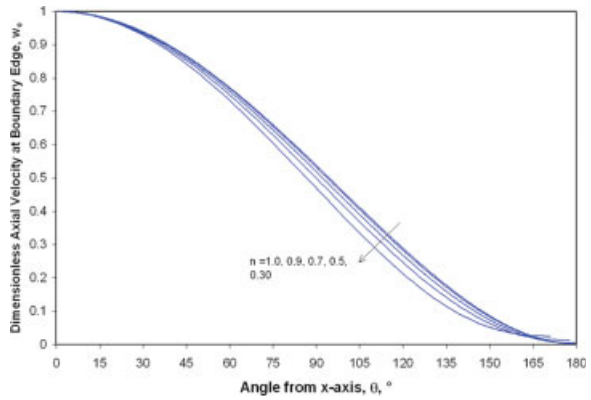

Figure 5. Dimensionless axial velocity at the outer edge of the boundary layer, w_o.

[Color figure can be viewed in the online issue, which is available at www.interscience.wiley.com.]

in which

$$\beta = \frac{2}{\pi}\int_0^{\pi} w_o \sin^2\theta d\theta \tag{64}$$

$$\gamma = \frac{3}{\pi}2^{-(n+2)/(n+1)}\int_0^{\pi} w_o \delta_o d\theta \tag{65}$$

Equation 63 indicates that once the flow field (w_o, δ_o, and S_o) are solved, the term (v_m/w_{10}) can be determined for a given Dean number, D_e, since β and γ can be calculated from the numerical solution. Table 1 shows the solutions of (v_m/w_{10}) for various D_e and n values.

Based on Table 1, the following empirical correlation can be developed:

$$\frac{v_m}{w_{10}} = c_1 + c_2 \ln D_e + c_3 n + c_4 (\ln D_e)^2 + c_5 n^2 + c_6 n \ln D_e \tag{66}$$

where $c_1 = 0.156898$, $c_2 = 0.0851820$, $c_3 = 0.0188959$, $c_4 = -0.00715958$, $c_5 = -0.152792$, and $c_6 = 0.0309871$.

For each value of n, an α value can be calculated through Eq. 53. α can then be correlated with n:

$$\alpha = [a' + b' \ \ln(n)]^2 \tag{67}$$

in which $a' = 0.669734019$, and $b' = -0.203276681$.

Let $Y = (v_m/w_{10})$, then the Fanning friction factor can be written as:

$$f = 2^{n/(n+1)} \alpha D_e^{-1/(n+1)} \left(\frac{a}{R}\right)^{1/2} Y^{-3n/(n+1)} \tag{68}$$

where,

$$Y = c_1 + c_2 \ln D_e + c_3 n + c_4 (\ln D_e)^2 + c_5 n^2 + c_6 n \ln D_e \tag{69}$$

Since the generalized Reynolds number has been widely used for non-Newtonian fluids, we introduced the following generalized Dean number based on generalized Reynolds number:

$$N_{DNg} = N_{Reg}(a/R)^{1/2} \tag{70}$$

It can then be shown that

$$D_e = 2^{3(n-1)} \left(\frac{3n+1}{4n}\right)^n N_{DNg} \tag{71}$$

where N_{Reg} is the generalized Reynolds number. Therefore, for a power law fluid with the rheological parameters (n and K_p) known, the Fanning friction factor through CT can easily be calculated using Eqs. 68–71.

As the friction factor correlation is a fit of a convenient functional form to the numerical computations, the use of such correlation must be strongly restricted to the conditions for which the correlation was developed, i.e., $0.25 \le n \le 1$ and $50 \le 2^{3(n-1)}[(3n+1)/(3n)]N_{DNg} \le 650$. Application of this correlation out of these ranges is not recommended.

Table 1. Values of (v_m/w_{10}) Calculated Based on Numerical Solutions

	Flow Behavior Index													
D_e	0.25	0.3	0.35	0.4	0.45	0.5	0.55	0.6	0.65	0.7	0.75	0.8	0.85	0.9	0.95	1
50	0.3984	0.4082	0.4119	0.4145	0.4159	0.4158	0.4143	0.4116	0.4079	0.4037	0.3984	0.3927	0.3865	0.3800	0.3731	0.3659
100	0.4228	0.4324	0.4366	0.4399	0.4421	0.4429	0.4426	0.4412	0.4389	0.4361	0.4324	0.4282	0.4236	0.4186	0.4132	0.4074
150	0.4331	0.4425	0.4472	0.4508	0.4535	0.4548	0.4552	0.4546	0.4531	0.4510	0.4482	0.4449	0.4411	0.4369	0.4323	0.4274
200	0.4389	0.4483	0.4532	0.4571	0.4601	0.4618	0.4626	0.4625	0.4615	0.4600	0.4577	0.4550	0.4518	0.4482	0.4442	0.4398
250	0.4426	0.4521	0.4572	0.4613	0.4646	0.4665	0.4676	0.4679	0.4673	0.4661	0.4643	0.4620	0.4592	0.4560	0.4525	0.4485
300	0.4453	0.4548	0.4600	0.4643	0.4678	0.4699	0.4713	0.4718	0.4715	0.4707	0.4692	0.4672	0.4648	0.4619	0.4587	0.4550
350	0.4473	0.4568	0.4622	0.4666	0.4702	0.4725	0.4741	0.4748	0.4748	0.4742	0.4730	0.4713	0.4691	0.4665	0.4635	0.4601
400	0.4489	0.4584	0.4639	0.4684	0.4721	0.4746	0.4763	0.4773	0.4775	0.4770	0.4760	0.4745	0.4726	0.4702	0.4675	0.4643
450	0.4501	0.4597	0.4653	0.4699	0.4737	0.4763	0.4782	0.4792	0.4796	0.4794	0.4786	0.4773	0.4755	0.4733	0.4708	0.4678
500	0.4511	0.4608	0.4664	0.4711	0.4750	0.4777	0.4797	0.4809	0.4815	0.4813	0.4807	0.4796	0.4780	0.4760	0.4736	0.4708
550	0.4520	0.4617	0.4674	0.4722	0.4761	0.4789	0.4810	0.4824	0.4830	0.4830	0.4825	0.4815	0.4801	0.4783	0.4760	0.4734
600	0.4528	0.4624	0.4682	0.4730	0.4771	0.4799	0.4822	0.4836	0.4844	0.4845	0.4841	0.4833	0.4820	0.4802	0.4782	0.4756
650	0.4534	0.4631	0.4689	0.4738	0.4779	0.4809	0.4832	0.4847	0.4856	0.4858	0.4855	0.4848	0.4836	0.4820	0.4800	0.4776

Comparison with previous work

Comparison with the Ito, and Mashelkar and Devarajan Correlations (Newtonian Fluid). For $n = 1$ (the Newtonian fluid case), the Ito[10] correlation can serve as a good check for accuracy of the newly developed correlation.

Ito[10] correlation:

$$f = 1.654\left(\frac{a}{R}\right)^{1/2} N_{D_e}^{-1/2}\left[\left(1+\frac{1.729}{N_{D_e}}\right)^{1/2} - \frac{1.315}{N_{D_e}^{1/2}}\right]^{-3} \quad (72)$$

Mashelkar and Devarajan Correlation:

$$f = (9.069 - 9.438n + 4.374n^2)(a/R)^{0.5} D_e^{(-0.768+0.122n)} \quad (73)$$

Figure 7 shows the plots of Fanning friction factor versus Dean number (D_e) for Ito,[10] Mashelkar and Devarajan,[11] and the new correlation of this study at curvature ratio of 0.01. It can be seen that there is an excellent agreement between the new correlation and the Ito correlation. But, the Mashelkar and Devarajan correlation fails to closely match the Ito correlation. The deviation between the Mashelkar and Devarajan correlation, and the Ito correlation is 14–22%. This discrepancy was also pointed out previously by Hsu and Patankar,[13] and Mujawar and Rao.[14]

Comparison with Mashelkar and Devarajan Correlation (Non-Newtonian Fluid)

Mashelkar and Devarajan[11] correlation is the only available correlation based on the similar approach of approximate boundary layer analysis for non-Newtonian fluids and it has been referenced in literature.[15] Therefore, it would be useful to compare our result with this correlation.

Figure 8 compares the Mashelkar and Devarajan correlation and our new correlation for the conditions of $n = 0.6$ and curvature ratio = 0.01. It can be noted from the results of Figures 7 and 8 that as flow behavior index n decreases, the deviation between the new correlation and the Mashelkar and Devarajan correlation becomes greater than for Newtonian fluid. Figure 9 indicates that according to the Mashelkar and Devarajan correlation, the flow behavior index (n) almost

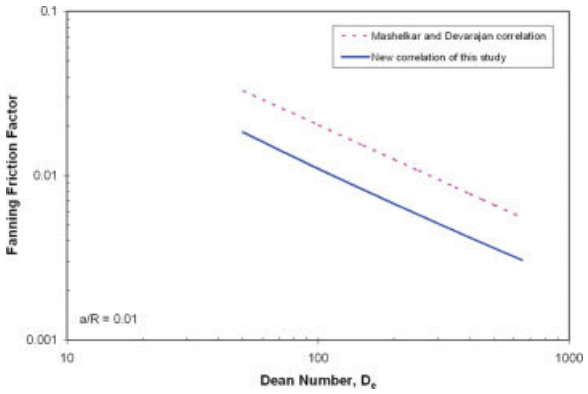

Figure 8. Comparison between the new correlation and the Mashelkar and Devarajan correlation (n = 0.6, a/R = 0.01).

[Color figure can be viewed in the online issue, which is available at www.interscience.wiley.com.]

has no effect on friction factor in CT. In contrast, according to the new correlation of this study, the friction factor decreases with decrease of flow behavior index, as shown in Figure 10. The discrepancy between the Mashelkar and Devarajan correlation and the new correlation could be due to errors in Mashelkar and Devarajan's equations (such as errors in Eqs. 58, 59, and 67 in Reference 11) and/or errors in numerical solutions.

Furthermore, in the work of Mashelkar and Devarajan, numerical solutions were obtained only for four n values (n = 1.0, 0.9, 0.75, and 0.5). Since their correlation could not match the Ito correlation even for $n = 1$, the correlation based on the four n values is questionable. Our new correlation not only matches the Ito correlation for $n = 1$, but it is also based on a much wider range of n, i.e., from 0.25 to 1.0 in steps of 0.05.

Comparison with experimental data

Experiments of fluid flow in CT have been conducted using a full-scale CT flow loop used for a joint industry project at the University of Oklahoma. The flow loop includes

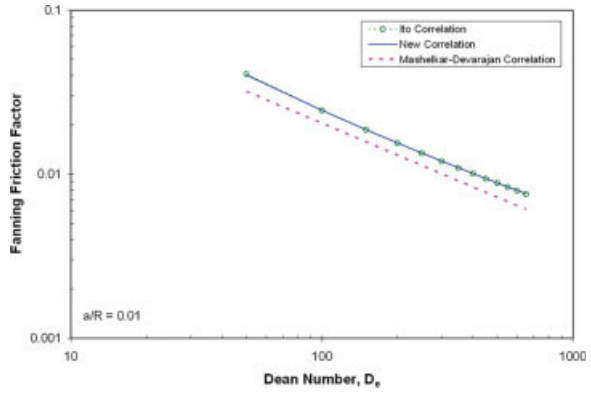

Figure 7. Comparison with Ito correlation (n = 1, a/R = 0.01).

[Color figure can be viewed in the online issue, which is available at www.interscience.wiley.com.]

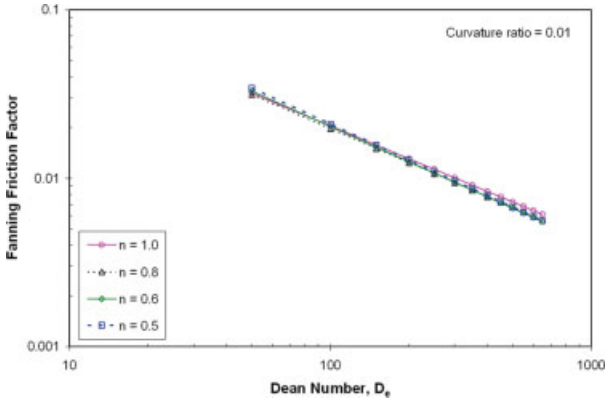

Figure 9. Effect of flow behavior index by Mashelkar and Devarajan correlation.

[Color figure can be viewed in the online issue, which is available at www.interscience.wiley.com.]

several reels of 25.4, 38.1, and 60.3-mm CT strings and straight tubing sections. The combinations of the three CT diameters, i.e., 25.4, 38.1, and 60.3-mm, and 3-reel drum diameters result in curvature ratio values of 0.0113, 0.0165, 0.0169, and 0.0185.

Fluids tested are typical drilling, completion, and stimulation fluids used in the oil and gas industry, including polymeric solutions and surfactant-based fluids. An oil-based drilling mud was also tested. These fluids are generally non-Newtonian and can be described by a power law model within the flow conditions investigated.

The primary measured data include the gross flow variables such as frictional pressure drops across different tubing sections at various flow rates. Rheological properties of fluids were evaluated using a Bohlin rheometer and a model 35 Fann viscometer. More detailed description of the experimental facility and experimental procedures can be found elsewhere.[16] The experimental data were used to evaluate the newly developed friction factor correlation.

Example 1—laminar flow of 7.2 kg/m^3 HPG in 60.3-mm CT

A 7.2 kg/m^3 HPG (hydroxypropyl guar) gel was pumped through the 304.8-m long, 60.3-mm diameter CT reel to investigate the laminar flow behavior of non-Newtonian fluid in CT. Rheological properties were evaluated using a Model 35 Fann viscometer: $n = 0.314$ and $K_v = 4.930$ Pa s^n. The experimental data and the predictions by our new correlation (Eq. 68) are shown in Figure 11. From the Srinivasan correlation,[17] the critical Reynolds number for Newtonian fluid in this coil is 5528. The critical Reynolds number for non-Newtonian fluids should be higher than this value.

It can be seen that the new laminar flow correlation of this study matches the experimental data reasonably well for the generalized Reynolds number up to 6000. Except the first data point, where the flow rate was very low, the absolute deviation varies from 0.01 to 9.3% with an average absolute deviation of 4.2%. At generalized Reynolds number greater than 6000, the correlation begins to deviate from the experimental data points. As generalized Reynolds number increases from 6558 to 9349, the friction factor predicted

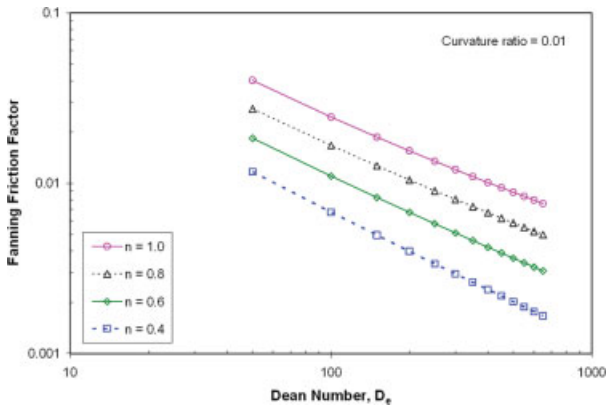

Figure 10. Effect of flow behavior index by the new correlation (*a*/*R* = 0.01).

[Color figure can be viewed in the online issue, which is available at www.interscience.wiley.com.]

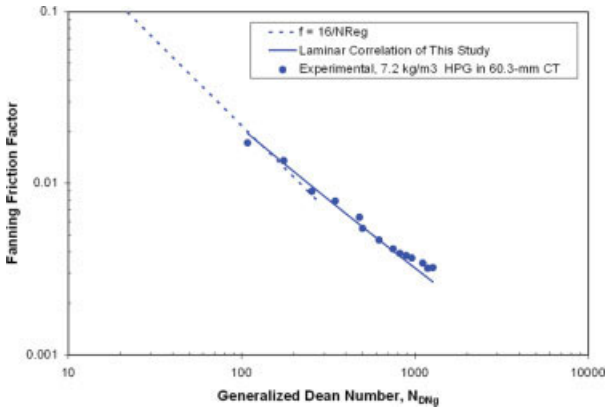

Figure 11. Friction factor of 7.2 kg/m^3 HPG in 304.8-m long, 60.3-mm OD coiled tubing (*a*/*R* = 0.0185).

[Color figure can be viewed in the online issue, which is available at www.interscience.wiley.com.]

from the correlation is 7.3–17.5% lower than the experimental data. Considering the high accuracies of the pressure transducers and the flowmeters, the random errors in measurement are much smaller than the deviations observed above (7.3–17.5%). Therefore, the reason for the deviation of the correlation with the friction factor data for Reynolds number greater than 6000 is most probably because the flow may have been in turbulent flow regime. Since one basic assumption of the boundary layer approximation approach is that the Dean number should be large, the new correlation is not recommended for $N_{DNg} < 100$. Fortunately, the flow conditions for field applications of CT would generally satisfy the requirement of large Dean number.

Example 2—3.6 and 4.8 kg/m^3 guar fluids in 60.3-mm CT

Figure 12 shows the plot of Fanning friction factor versus generalized Dean CT. It compares the experimental data and the predictions by the new correlation and by the Mashelkar

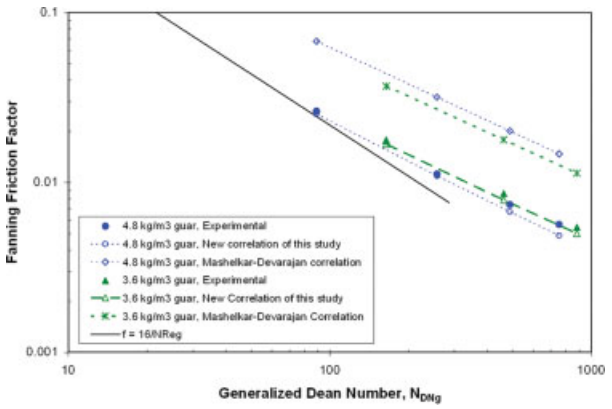

Figure 12. Comparison between experimental data and correlations (3.6 and 4.8 kg/m^3 guar in 304.8-m long, 60.3-mm OD coiled tubing (*a*/*R* = 0.0185)).

[Color figure can be viewed in the online issue, which is available at www.interscience.wiley.com.]

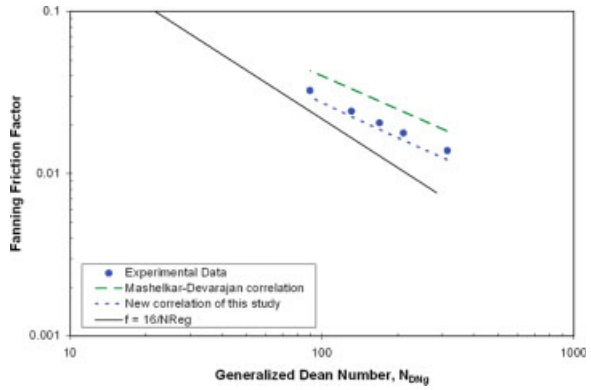

Figure 13. Comparison between experimental data and correlations (oil-based drilling mud in 304.8-m long, 60.3-mm OD coiled tubing, a/R = 0.0185).

[Color figure can be viewed in the online issue, which is available at www.interscience.wiley.com.]

and Devarajan correlation. The rheological properties of the guar fluids are: $n = 0.432$, $K_v = 1.066$ Pa s^n for 4.8 kg/m^3 guar solution, and $n = 0.527$, $K_v = 0.352$ Pa s^n for 3.6 kg/m^3 guar solution. It can be observed that there is a good agreement between the experimental data and the predictions by the new correlation of this study. It is found that the deviations between the predicted and experimental friction factors are generally within 10%. Unfortunately, the Mashelkar and Devarajan correlation predictions are much higher than the experimental data in this case.

Example 3—oil-based drilling mud in 60.3-mm CT

Figure 13 compares the experimental data of an oil-based drilling mud in 60.3-mm CT with predictions by the two correlations. The power law parameters of this oil mud are: $n = 0.689$, $K_v = 0.483$ Pa s^n. It is shown that the new correlation is very close to the experimental data, only underestimating the friction factors by about 10.0%. The Mashelkar and Devarajan correlation overpredicts the friction factors by about 37%.

Conclusions

(1) The boundary layer approximation method has been successfully applied to the theoretical and numerical analysis of laminar flow of power-law fluid in CT under conditions of large Dean numbers.

(2) A new friction factor correlation has been developed based on extensive numerical analysis. The new correlation, expressed in an empirical form of Fanning friction factor as function of generalized Dean number, curvature ratio, and flow behavior index, can be used in the hydraulics design of CT injection operations.

(3) There has been an excellent agreement between the new friction factor correlation and the experimental data obtained from experiments of typical drilling and completion fluids in the full-scale CT flow loop.

(4) The Mashelkar and Devarajan correlation was evaluated by comparing it with the experimental data, Ito correlation for $n = 1$ (Newtonian fluid), and the new correlation of this study. It was found that Mashelkar and Devarajan correlation failed to give any acceptable agreement with either the experimental data or the Ito correlation.

(5) The present work not only corrects the errors in the Mashelkar and Devarajan correlation, but also extends the range of applicability of the new correlation to fluids with flow behavior indices as low as 0.25, which would cover most fluids used in CT operations in the oil and gas industry as well as other industries.

Acknowledgments

The authors wish to thank the members of the Coiled Tubing Consortium for their continued support and the research team at the Well Construction Technology Center for their assistance during this research.

Notation

a = radius of coiled tubing
a' = coefficient in Eq. 67
a/R = curvature ratio
b' = coefficient in Eq. 67
c_1–c_6 = correlation coefficients in Eq. 66
C = axial pressure gradient
d = pipe diameter
D_e = Dean number, $(2a)^n v_m^{2-n}\rho/K$
f = Fanning friction factor
F = function defined in Eq. 11
$g(\eta)$ = function defined in Eq. 41
$h(\eta)$ = function defined in Eq. 42
$k(\eta)$ = function define in Eq. 43
K = consistency index of power law model
K_p = consistency index from pipe viscometer, Pa·s^n
K_v = consistency index from Fann viscometer, Pa·s^n
n = flow behavior index, dimensionless
N_{DNg} = generalized Dean number, Eq. 70
N_{Re} = Reynolds number $(=\rho dv/\mu)$
N_{Reg} = generalized Reynolds number$(=d^n v^{2-n}\rho/K_p 8^{n-1})$
N'_{Reg} = defined in Eq. 49
p = pressure
r = radial coordinate
R = radius of coiled tubing reel
S = v-component velocity factor, Eq. 39
S_o = dimensionless S, Eq. 46
S_{o1}, S_{o3} = S_o expansion coefficients, Eq. 55
u = velocity component in r direction
v = velocity component in θ direction
v_m = mean velocity
w = velocity component in ϕ direction
w_1 = axial velocity component at the edge of the boundary layer
w_{10} = value of w_1 at $\theta = 0$
w_o = dimensionless axial velocity at the boundary layer edge
w_{o2} = coefficient of w_o expansion
x = horizontal Cartesian coordinate
y = vertical Cartesian coordinate
α = function defined in Eq. 53
δ = boundary layer thickness
δ_o = dimensionless boundary layer thickness
δ_{o1}, δ_{o2} = coefficients of δ_o expansion, Eq. 54
θ = angular coordinate
η = dimensionless coordinate $(=\xi/\delta)$
ψ = stream function
μ = viscosity
$\xi = a - r$
ρ = fluid density
τ = shear stress
ϕ = axial angular coordinate
$\dot{\gamma}$ = shear rate

Subscripts

rr = in r direction in plane normal to r
$R\theta$ = in θ direction in plane normal to r
$r\phi$ = in ϕ direction in plane normal to r
$\theta\theta$ = in θ direction in plane normal to θ

Literature Cited

1. Dean WR. Note on the motion of fluid in a curved pipe. *Philos Mag*. 1927;20:208–223.
2. Dean WR. The streamline motion of fluid in a curved pipe. *Philos Mag*. 1928;30:673–693.
3. Zhou Y, Shah SN. Fluid flow in coiled tubing: a literature review and experimental investigation. *J Can Pet Technol*. 2004;43:52–61.
4. Adler M. Flow in curved pipes. *Z Angew Math Mech*. 1934;14:257–275.
5. McConalogue DJ, Srivastava RS. Motion of a fluid in a curved tube. *Proc R Soc London Ser A*. 1968;307:37–53.
6. Greenspan D. Secondary flow in a curved tube. *J Fluid Mech*. 1973;57:167–176.
7. Collins WM, Dennis CR. The steady motion of a viscous fluid in a curved tube. *Q J Mech Appl Math*. 1975;28:133–156.
8. Barua SN. On secondary flow in stationary curved pipes. *Q J Mech Appl Math*. 1963;16:61–77.
9. Mori Y, Nakayama W. Study on forced convective heat transfer in curved pipes (1st Report). *Int J Heat mass Transfer*. 1965;8:67–82.
10. Ito H. Laminar flow in curved pipes. *Z Angew Math Mech*. 1969;49: 653–663.
11. Mashelkar RA, Devarajan GV. Secondary flows of non-Newtonian fluids, Part I: Laminar boundary layer flow of a generalized non-Newtonian fluid in a coiled tube. *Trans Inst Chem Eng*. 1976;54: 100–107.
12. Devarajan GV. *Secondary flows of non-Newtonian fluids*. PhD Dissertation. Salford, UK: University of Salford, 1975.
13. Hsu CF, Patankar SV. Analysis of laminar non-Newtonian flow and heat transfer in curved tubes. *AIChE J*. 1982;28:610–616.
14. Mujawar BA, Rao MR. Flow of non-Newtonian fluids through helical coils. *Ind Eng Chem Process Des Dev*. 1978;17:22–27.
15. Perry RH. *Perry's Chemical Engineers' Handbook*, 7th ed. New York, NY: McGraw-Hill, 1999: Chapter 5.
16. Zhou Y. *Theoretical and experimental studies of power-law fluid flow in coiled tubing*. PhD Dissertation. Norman, OK: University of Oklahoma, 2006.
17. Srinivasan PS, Nandapurkar SS, Holland FA. Friction factors for coils. *Trans Inst Chem Eng*. 1970;48:T156–T161.

Manuscript received Oct. 27, 2006, and revision received May 24, 2007.